molecular pharmaceutics

Article

pubs.acs.org/molecularpharmaceutics

Nanopolymeric Micelle Effect on the Transdermal Permeability, the Bioavailability and Gene Expression of Plasmid

Yaw-Chong Tong,[†] Ting-Yu Yu,[†] Shwu-Fen Chang,[‡] and Jiahorng Liaw*[,†]

[†]College of Pharmacy and [‡]Graduate Institute of Medical Sciences, College of Medicine, Taipei Medical University, Taipei, Taiwan

ABSTRACT: This study attempts to investigate the transdermal permeability, the bioavailability and gene expression of plasmid formulated with nonionic poly(ethylene oxide)-poly(propylene oxide)-poly(ethylene oxide) (PEO-PPO-PEO) polymeric micelles (PM). Dynamic light scattering (DLS) and atomic force microscopy (AFM) were used to analyze the PM formulated pCMV-*Lac* Z (P/PM) containing the gene for β-galactosidase (β-Gal) driven by cytomegalovirus early promoter. Franz diffusion cell was used for *in vitro* transdermal permeability analysis. Real-time PCR was used to quantify the permeated plasmid *in vitro* and *in vivo*. β-Gal activity assay was performed to evaluate transgene expression *in vivo*. The size of P/PM was ~50 nm with round shape. PM significantly enhanced the *in vitro* transdermal permeability of plasmid in a direction- and temperature-dependent manner. Following transdermal application of P/PM, higher area under the curve ($AUC_{P/PM}$: 98.34 h·ng/mL) and longer half-life of plasmid were detected compared with that of plasmid alone (AUC_P: 10.12 h·ng/mL). Additionally, the β-Gal activity was significantly increased in skin, stomach, brain and spinal cord at both 48 and 72 h after P/PM application and in testis and spleen at 72 h postapplication. In conclusion, PM formulation enhanced the permeation of plasmid through skin into blood circulation, increasing its absorption and the transgene expression in various tissues.

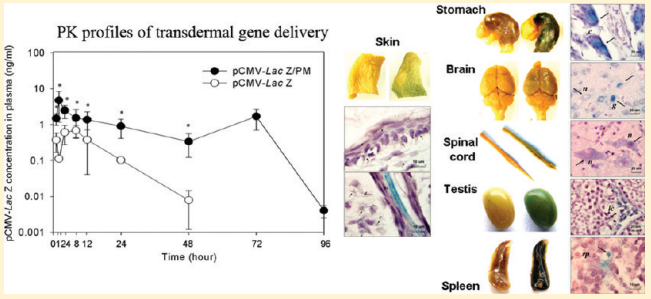

KEYWORDS: *transdermal permeability, nanocarrier, polymeric micelles*

INTRODUCTION

The skin is an attractive delivery route, primarily because of its being the largest surface in the body and relatively easy to access and monitor.[1] Topical administration of DNA has recently received great attention in the fields of cutaneous and local gene therapies.[1−7] In the past, topical administration of plasmid with liposomes to predepilated mouse skin or hairless rat pup resulted in a maximal transgene expression detected at 24 h postadministration but declined at 48 h, and the expression was distributed in the epidermis, dermis and hair follicles.[1−3] Although the low penetration efficacy of topically applied DNA through skin is a major concern, the transgene expression was detected when naked DNA was topically applied to skin with puncture-mediated instillation, gene gun or electric pulse devices, or to damaged skin.[4−7] However, less invasive approaches will be more attractive to achieve both therapeutic efficacy and patient acceptance.

Recently, transdermal application has been an emerging route for systemic gene delivery since increasing evidence imply that exogenous DNA may permeate the skin, reaching the underlying tissues and even enter the blood circulation.[7−9] Kang et al.[8] reported that, following topical application of naked DNA to the skin of hairless mice at a relatively higher dosage of 300 μg/mouse, which was about 3- to 10-fold the amount used in other studies, plasmid DNA was detected in blood starting at 1 h postapplication and up to 24 h,[7,10] indicating the success of DNA delivery across the skin tissue. However, a low absolute bioavailability (0.18%) of the delivered DNA was reported and reasoned by the presence of the stratum corneum structure in the skin, which were well-known as a rate-controlling barrier for skin permeation.[11,12] Therefore, improving the efficiency of plasmid passing through an intact skin tissue *via* nanopathway of the stratum corneum may be one way to increase the absorption and the bioavailability of plasmid for systemic delivery.[13]

Nano polymeric particles have several advantages for dermal and transdermal deliveries, including the increased flux, sustained release and enhanced bioavailability of formulated drugs and genes.[3,13−16] Among the polymeric carriers, a nonionic PEO-PPO-PEO triblock copolymer has been widely used in the fields of medicine, pharmaceutics, ophthalmics and cosmetics with its relatively low toxicity.[17−21] The hydrophilic PEO corona and the hydrophobic PPO core of the copolymer allow it to self-assemble to nanosized polymeric micelles (PM) with higher resistance to protein/serum absorption and enzymatic digestion.[17−19,22] In addition, formulations with this triblock copolymer give rise to a more stable and sustained drug release with longer circulation time after iv injection, as well as oral or transdermal patch delivery.[23−26] Therefore, the

Received: July 7, 2011
Revised: November 2, 2011
Accepted: December 5, 2011
Published: December 5, 2011

dx.doi.org/10.1021/mp200342h | *Mol. Pharmaceutics* 2012, 9, 111−120

aim of this study was to evaluate the feasibility of the nanocarrier, PM, to enhance transdermal permeability of plasmid and to investigate the pharmacokinetics and gene expression of PM-formulated pCMV-*Lac* Z (P/PM) after *in vivo* topical transdermal administration. We detected an enhanced transdermal permeability of plasmid after PM formulation, and the transdermal permeation may involve an energy-dependent process. *In vivo* topical transdermal administration of P/PM, a higher area under the curve (AUC) and longer half-life of the plasmid were detected compared with those detected in animals receiving pCMV-*Lac* Z alone. The β-Gal activity was significantly increased in skin, stomach, testis, spleen and distant organs like brain and spinal cord.

MATERIALS AND METHODS

PEO-PPO-PEO copolymer with an average molecular weight of 8,400 (Pluronic F68) was obtained from the BASF Corporation (Ludwigshafen, Germany). All other chemicals were analytical reagent grade and used without further purification. Animal experiments were approved by the Laboratory Animal Research Committee of Taipei Medical University. The nude mice (BALB/cAnN.Cg-*Foxn1*^{nu}/CrlNarl, male, 6 to 8 weeks old) used in the *in vitro* permeation and *in vivo* topical transdermal delivery studies were purchased from the National Laboratory Animal Center (Taipei, Taiwan) and maintained under specific pathogen free condition.

Preparation and Characterization of Plasmid DNA and Plasmid/Polymer. The pCMV-*Lac* Z plasmid, containing the *Lac* Z gene for β-galactosidase (β-Gal), was constructed such that *Lac* Z expression was driven by the cytomegalovirus early promoter.[22,26] Plasmid was amplified in the *Escherichia coli* host DH5α strain and was purified by equilibrium centrifugation in a CsCl−EtBr gradient.[27] The purity and stability of plasmid preparations were confirmed by agarose gel electrophoresis followed by ethidium bromide staining, and the DNA concentration was measured by UV absorption at 260 nm. In this study, different concentrations (0.01, 0.1 and 5%) of polymer were freshly prepared by a weight percentage basis as described in previous studies.[21,22,24] The assembly of PM was previously confirmed by a fluorescence probe, pyrene, and the critical micelle concentration (CMC) of polymeric micelles was above 0.1%.[22,24] After plasmid/polymer was mixed with different concentrations (0.01, 0.1 and 5%) of polymer with plasmid (0.4 μg/μL), the amount of plasmid encapsulated in the PM was calculated by measuring the difference between the total amount of plasmid (P) added in the PM preparation and the amount of non-entrapped plasmid remaining in the aqueous solution. After the complex was formed at ambient temperature for 2 h, two separated peaks of the complexes P/PM and non-entrapped plasmid (P) were determined by HPLC analysis (TSK-GEL G5000 PWXL column, 0.7 mL/min flow rate of water (pH 4.5) mobile phase). Loading efficiency of P/PM [(total amount of plasmid − non-entrapped plasmid)/total amount of plasmid)] was found to be 58 ± 3%. In addition, similar results were confirmed by collection of two separated fractional peaks and were quantified by real time-PCR.

The particle size and zeta potential of plasmid (0.4 μg/μL in H_2O) alone, polymer at various concentrations (0.01, 0.1 and 5%) and plasmid/polymer (0.4 μg/μL of plasmid DNA in 0.01, 0.1 or 5% of polymer) were measured by quasi-elastic laser dynamic light scattering (DLS) (Zetasizer 3000, Malvern Instruments, Malvern, U.K.) with an assumed refractive index ratio of 1.33 and viscosity of 0.88. All measurements were performed at 25 °C at a measurement angle of 90°, and results are presented as mean ± SD.[21,22,24] Three microliters of plasmid (0.4 μg/μL in H_2O), PM (5%) or P/PM (0.4 μg/μL DNA in 5% PM) was placed on a mica surface with no further treatment for atomic force microscopy (AFM) (diCP-II; Digital Instruments/Veeco Metrology Group, Santa Barbara, CA) observation with constant tapping mode. The cantilevers were standard NSC15/AIBS silicon single-rectangular cantilever (230 μm) (MikroMasch, Estonia), and the constant force mode was used with a resonant scan frequency of 328 kHz. All images were collected within 1.0 × 1.0 μm^2 areas.

***In Vitro* Membrane Permeation of Plasmid DNA and Nanoparticles.** In order to study the effect of PM on plasmid permeation, a Franz cell with a cellulose membrane (pore size, 0.2 μm; diffusion area, 0.627 cm^2, Pall Life Sciences, USA) was used for the *in vitro* permeated study as described previously.[21,24] Additionally, to compare the effect of particle size on the transport profile, polystyrene nanoparticles with a mean diameter of 40 or 100 nm (FluoSpheres, Molecular Probes, Oregon, USA; nanoparticles, containing fluorescein 5-isothiocyanate, are coated with a relatively hydrophilic polymer containing multiple carboxylic acids) was used for the *in vitro* release study as described previously.[28] Plasmid, P/PM (500 μL of 0.4 μg/μL of plasmid or P/PM) or nanoparticles (500 μL of 0.025%) were placed in the donor compartment, and 6 mL of pH 7.4 phosphate buffer solution (PBS) was placed in the receiver compartment. The diffusion cells were maintained at 37 °C in a water bath (SR70, Shimaden, Tokyo, Japan), and stirring was set at 700 rpm throughout experiment. Samples were withdrawn from the receiver compartments at fixed intervals (5, 15, 30, 60, 120, and 240 min) and replaced with an equal volume of prewarmed PBS. The permeated plasmid DNA was analyzed by the real-time PCR, and the permeated nanoparticles were analyzed by a fluorescence spectrophotometer F-4500 (Hitachi, Tokyo, Japan) with standard curves.

***In Vitro* Skin Permeation of Plasmid, Plasmid/Polymer and Nanoparticles.** Fresh samples of abdominal side of nude mouse skin were removed and mounted carefully between two compartments of the Franz cell (with 0.627 cm^2 of diffusion area) with a rigid clamp.[24] Solution in 100 μL of volume containing plasmid (0.4 μg/μL in H_2O) or plasmid/polymer (0.4 μg/μL DNA in 0.01, 0.1 or 5% of polymer) or 500 μL of nanoparticles with diameter of 40 nm (0.025%) was placed in the donor compartment. The receiver compartment was filled with 6 mL of PBS (pH 7.4) and maintained at 37 °C (or 20 °C, 4 °C) in a water bath (SR70, Shimaden, Tokyo, Japan) with 700 rpm stirring throughout the experiment. Aliquots (200 μL) from solution in the receiver compartment were collected at indicated time intervals and replaced with an equal volume of prewarmed PBS (or precooled PBS). Additionally, after *in vitro* skin permeation of 40 nm nanoparticles, cryosections (10 μm) of the OCT (Sakura Finetek U.S.A., Torrance, CA, USA)-embedded, paraformaldehyde fixed permeated skins were washed and observed using a laser confocal microscope (TCS SP5 confocal spectral microscope imaging system, Leica, Germany). Moreover, the skin was pretreated with sodium azide (150 mM, 15 min) (Sigma-Aldrich, Dorset, U.K.), an inhibitor of ATP synthesis,[29,30] for evaluating whether the permeation of plasmid, P/PM or nanoparticles involved an energy-dependent process. The permeated plasmid DNA was analyzed by real-time PCR, and the permeated nanoparticles were analyzed by a fluorescence spectrophotometer. The apparent permeability coefficient (P_{app}) was calculated

according to the following equation as described previously.[24] $P_{app} = (dC/dt)V/A \times C_0$, where $V(dC/dt)$ is the steady state rate of plasmids or nanoparticles appearing in the receiver chamber after the initial lag time, C_0 is the initial concentration of plasmids or nanoparticles in the donor chamber, and A is the area of skin tissue exposed (0.627 cm^2).

***In Vivo* Transdermal Application of Plasmid or P/PM on Nude Mice.** Animals received food and water *ad libitum*. Before application of plasmid or P/PM, mice were intraperitoneally anesthetized with a single dose of pentobarbital (70 mg/kg) for cannulated jugular vein in nude mouse. A 1 cm incision was made at the ventral neck to expose the jugular vein, which was then catheterized using a polyurethane catheter and fixed in place. The plasmid or P/PM solution (100 μL of 0.4 $\mu g/\mu L$ in H_2O or 5% PM) was transdermally applied to the skin on the abdominal side with an area of 2 × 2 cm^2 with a cellulose backing membrane in 48 h. At 1, 2, 4, 8, 12, 24, 48, 72, 96, and 120 h postadministration, 50 μL of blood was sampled from cannulated jugular vein and centrifuged at 13,200 rpm for 10 min at 4 °C. The amounts of plasmid DNA in blood were further purified by phenol/chloroform extraction, ethanol precipitated and analyzed by real-time PCR.[21,22]

Real-Time PCR Analysis of the Permeated Plasmid *in Vitro* and *in Vivo*. Real-time PCR was performed using SYBR Green PCR Master Mix in an ABI PRISM 7300 Sequence Detection System (Applied Biosystems 7300 System Sequence Detection System (SDS) software version 1.3), and the level of plasmid DNA was determined by the absolute quantification method according to our previous study.[21,22] The primers for *Lac* Z (forward, 5′-CTACACCAACGTAACCTATCCC-3′, and reverse, 5′-TTCTCCGGCGCGTAAAAATGCG-3′) were used. The conditions for the PCR were as follows: 50 °C for 2 min, 95 °C for 10 min and 40 cycles of 95 °C for 15 s and 60 °C for 1 min. At the end of the PCR cycles, amplification specificity was confirmed by a dissociation curve analysis and the products were separated on a 3% agarose gel and stained with ethidium bromide for visual confirmation of the PCR product.

Pharmacokinetic Profile of the Plasmid in Plasma Following Transdermal Application. The plasmid concentrations in plasma after *in vivo* transdermal application of plasmid alone or P/PM were analyzed by the noncompartmental analytical model (WinNonlin 4.1, Pharsight, CA, USA) to obtain the area under the curve ($AUC_{0\to\infty}$) and half-life of plasmid.

Determination of β-Galactosidase (β-Gal) Activity. β-Gal activity was quantified using the Galacto-Light Plus System (Applied Biosystems, Foster City, CA, USA) according to the manufacturer's protocol as described in the previous study.[22] Briefly, mice were sacrificed at 48, 72, or 96 h post-topical transdermal application, and the tissues including abdominal skin, lung, heart, liver, stomach, duodenum, kidney, testis, brain and spinal cord were removed immediately, washed twice with PBS and then homogenized in lysis buffer. The resulting lysates were frozen at −80 °C. Following thawing and centrifugation at 13,200 rpm for 10 min at 4 °C, 20 μL of the supernatant was analyzed for chemiluminescence with a Veritas microplate luminometer (Turner BioSystems, Inc., Sunnyvale, CA, USA) with the addition of diluted Galacton-Plus reaction buffer and incubation at room temperature for 45 min. Total tissue protein was measured using the *DC* protein assay kit (BioRad, Hercules, CA, USA), which was used to normalize β-Gal activity in each sample.

The histological localization of β-Gal activity was determined with X-Gal (5-bromo-4-chloro-3-indolyl-β-D-galactoside) (Invitrogen Life Technologies, Carlsbad, CA, USA).[22,26] Tissues were washed with PBS twice and fixed with 4% paraformaldehyde at 4 °C for 90 min, and then rinsed with PBS. The tissue was then incubated with 10 mM $K_4Fe(CN)_6$, 10 mM $K_3Fe(CN)_6$, 0.01% sodium deoxycholate, 0.02% Nonidet-40 (NP-40), and 2 mM $MgCl_2$ in PBS solution containing 1 mg/mL of X-Gal substrate, pH 7.4, at 37 °C for 48−72 h. Cryosections (10 μm) of the OCT (Sakura Finetek U.S.A., Torrance, CA, USA)-embedded stained tissues were washed in an acetone−methanol (1:1) solution, and then stained with hematoxylin−eosin for histological assessment. β-Gal activity was visualized as the appearance of green-blue color under a microscope (Olympus BX-40, Japan).

Statistic Analysis. All results were presented as mean ± SEM. Statistical comparisons were calculated by ANOVA tests followed by post hoc testing with Dunnett's, Newman−Keuls, or Bonferroni multiple-comparison method for comparison of all groups with the control group, evaluation of the difference among groups, or comparison of designated pairs of groups at a 95% confidence level.

RESULTS

Characterization of PM Formulated Plasmid. The particle sizes of pCMV-*Lac* Z, polymer at different concentrations (0.01, 0.1 and 5%) and pCMV-*Lac* Z formulated with polymer were measured by dynamic light scattering (DLS), and the results are shown in Table 1. At concentration above the CMC (0.1%) as our previous studies,[22,24] the particle sizes of 5% polymer were significantly larger than those of polymer at 0.01 and 0.1% concentrations, and it was similarly known that this self-assembly of polymers formed the polymeric micelles.

Table 1. Particle Size and Zeta Potential of Polymer, Plasmid and Plasmid/Polymer[a] and Apparent Permeability Coefficient (P_{app}) of Plasmid and Plasmid/Polymer on Nude Mouse Skin[b]

	particle size (nm)	zeta potential (mV)	P_{app} ($\times 10^{-11}$ cm/s)
polymer			
0.01%	7.1 ± 2.1	−2.1 ± 0.3	
0.1%	9.5 ± 2.9	−2.1 ± 0.6	
5%	31.4 ± 6.2[c,d]	−2.7 ± 0.2	
pCMV-*Lac* Z	66.8 ± 3.5	−56.7 ± 0.8	3.4 ± 0.8
pCMV-*Lac* Z/0.01%	72.1 ± 4.9	−56.6 ± 0.7	4.8 ± 0.9
pCMV-*Lac* Z/0.1%	47.6 ± 7.5[e,f]	−15.3 ± 8.8[e,f]	4.1 ± 1.0
pCMV-*Lac* Z/5%	51.1 ± 6.3[e,f]	−1.3 ± 0.7[e,f,g]	11.2 ± 2.7[e,f,g]

[a]Plasmid (0.4 $\mu g/\mu L$ in H_2O) alone, polymer at various concentrations (0.01, 0.1 and 5%) and polymer containing plasmid (0.4 $\mu g/\mu L$ of plasmid in 0.01, 0.1 or 5%) were measured. Results are expressed as the mean with standard deviation (n = 6). [b]Plasmid or plasmid/polymer (100 μL of 0.4 $\mu g/\mu L$ of plasmid in H_2O or 0.01%, 0.1%, 5% polymer) in the donor compartment of Franz cells (n = 6−9). [c]Denotes a significant difference ($P < 0.05$) compared with 0.01%. [d]Denotes a significant difference ($P < 0.05$) compared with 0.1%. [e]Denotes a significant difference ($P < 0.05$) compared with pCMV-*Lac* Z. [f]Denotes a significant difference ($P < 0.05$) compared with pCMV-*Lac* Z/0.01%. [g]Denotes a significant difference ($P < 0.05$) compared with pCMV-*Lac* Z/0.1%.

dx.doi.org/10.1021/mp200342h | *Mol. Pharmaceutics* 2012, 9, 111−120

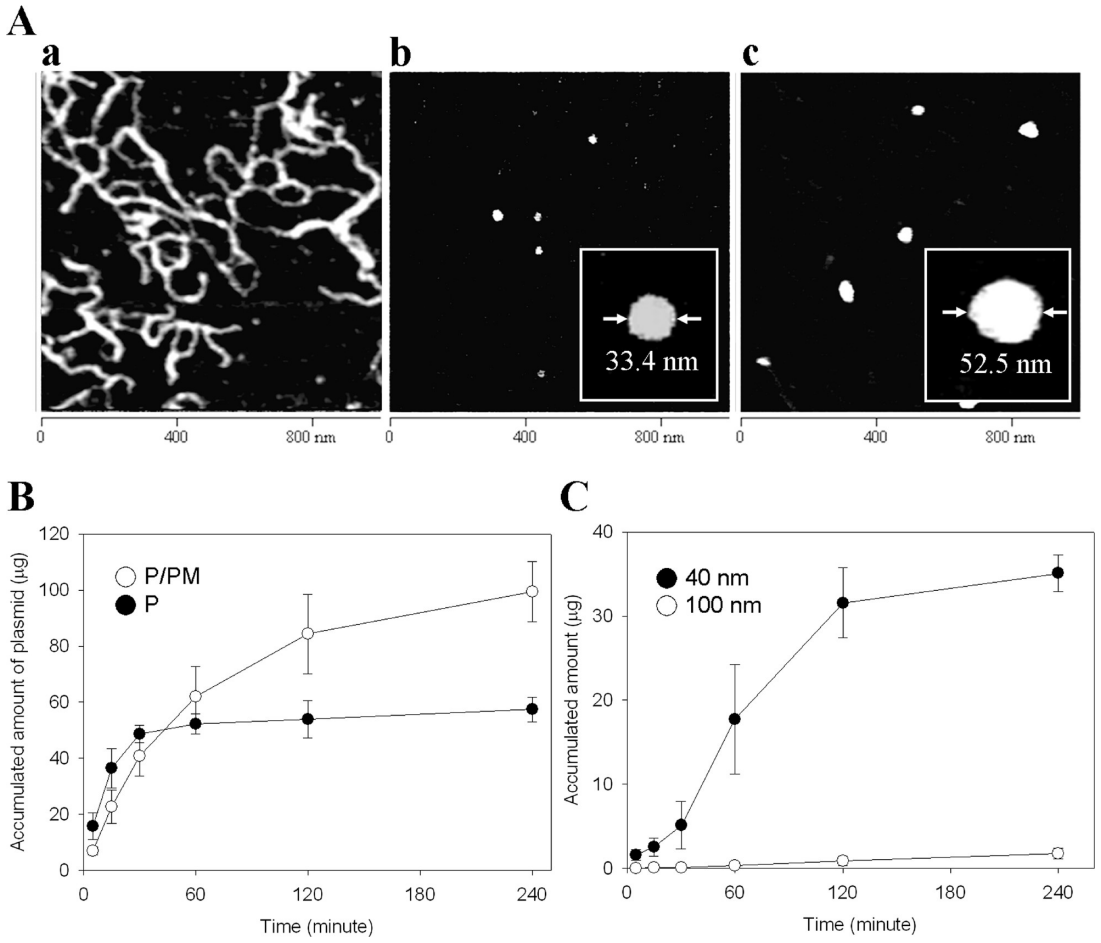

Figure 1. AFM images and release profile of pCMV-*Lac* Z, pCMV-*Lac* Z/PM, 40 and 100 nm nanoparticles. (A) AFM images of pCMV-*Lac* Z (a), PM (b), and pCMV-*Lac* Z/PM (c) (3 μL of 0.4 μg/μL plasmid with 5% PM solution on a mica surface). (B) Effect of PM on pCMV-*Lac* Z (P) permeation in a cellulose membrane (mean ± SEM, $N = 6$). (C) Effect of 40 and 100 nm FluoSpheres particle permeation in a cellulose membrane (mean ± SEM, $N = 6$).

Table 2. Apparent Permeability Coefficient (P_{app}) of pCMV-*Lac* Z, pCMV-*Lac* Z/PM and 40 nm Nanoparticles Permeating Nude Mouse Skin at Different Direction, Temperature (37 °C, 20 °C and 4 °C) and Sodium Azide Treatment[a]

	P_{app} (cm/s)				
	37 °C				
	sc[b] to dermis[c]	sc. to dermis/NaN_3[d,e]	dermis to sc[f]	20 °C	4 °C
pCMV-*Lac* Z[g]	3.4 ± 0.8	nd[h]	1.9 ± 1.3	1.6 ± 0.7	1.1 ± 0.6[i]
pCMV-*Lac* Z/PM[g]	11.2 ± 2.7[i]	nd[h]	0.2 ± 0.1[j]	4.0 ± 1.2[j]	1.7 ± 1.2[j]
40 nm nanoparticles[k]	154.3 ± 10.8	nd[h]	6.4 ± 0.9[l]	26.8 ± 3.1[l]	4.9 ± 0.7[l]

[a]Plasmid, plasmid/PM (100 μL of 0.4 μg/μL of plasmid in H_2O or 5% PM) or nanoparticles with diameter of 40 nm (500 μL of 0.025%) in the donor compartment of Franz cells. Data from 6 to 9 experiments and expressed as mean ± SEM. [b]Stratum corneum. [c]The stratum corneum to dermis meant that the plasmid permeated the skin from stratum corneum to the dermis of skin. [d]NaN_3: Sodium azide. [e]The stratum corneum to dermis/sodium azide was represented that the plasmid permeated the skin from stratum corneum to the dermis of skin with preincubated with 150 mM sodium azide. [f]The dermis to stratum corneum meant that the plasmid permeated the skin from dermis to stratum corneum. [g]The unit of P_{app}: $\times 10^{-11}$ cm/s. [h]Not detected. [i]Denotes a significant difference ($P < 0.05$) compared with pCMV-*Lac* Z of stratum corneum to dermis at 37 °C. [j]Denotes a significant difference ($P < 0.05$) compared with pCMV-*Lac* Z/PM of stratum corneum to dermis at 37 °C. [k]The unit of P_{app}: $\times 10^{-9}$ cm/s. [l]Denotes a significant difference ($P < 0.05$) compared with 40 nm nanoparticles of stratum corneum to dermis at 37 °C.

The particle size of pCMV-*Lac* Z in solution was 66.8 ± 3.5 nm and significantly decreased to the range of 47.6−51.1 nm upon formulation with various concentrations of polymer (above the CMC: 0.1 and 5%) (Table 1). The zeta potential of pCMV-*Lac* Z alone was −56.7 ± 0.8 mV (Table 1), and it was about −2 mV for 0.01, 0.1 or 5% polymer alone. Although the zeta potential of pCMV-*Lac* Z formulated with 0.01% polymer (−56.6 ± 0.7 mV) was similar to that of plasmid alone, the significant increase of the zeta potential to −15.3 ± 8.8 and −1.3 ± 0.7 mV was detected when plasmid DNA formulated with 0.1 and 5% polymer, respectively.

To further observe the PM-formulated plasmid, AFM was used. Results revealed that both PM and P/PM (Figures 1Ab and 1Ac) have round-shaped appearance and each had particle size similar to that detected by the DLS method. The permeating profiles of plasmid in H_2O or PM through cellulose

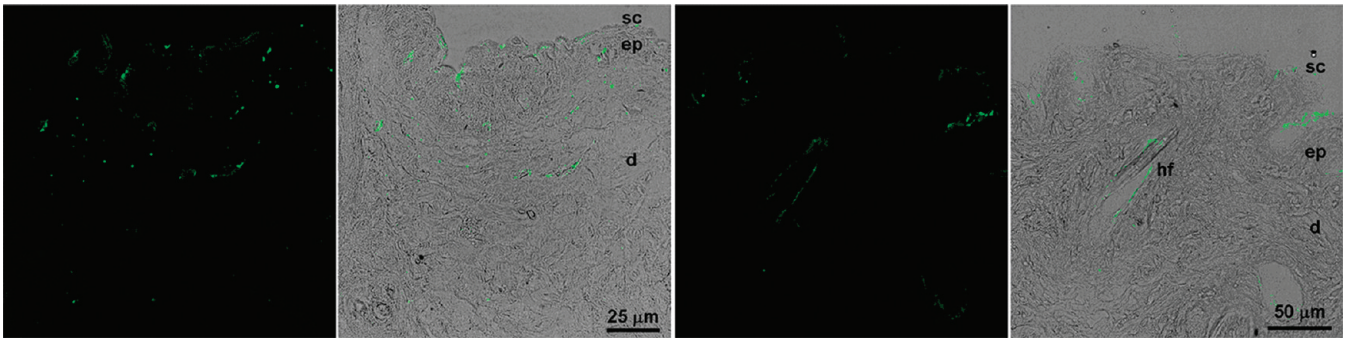

Figure 2. 40 nm nanoparticles penetrate *via* the stratum corneum and epidermis into the dermis of skin. Laser confocal microscopy was performed on cryosections of nude skin permeated with 40 nm nanoparticles (FluoSpheres with fluorescein 5-isothiocyanate (FITC)) *in vitro*. Image overlay was used to localize the fluorescence signal (green) on the tissue sections. Laser confocal microscopy revealed fluorescence signals (40 nm nanoparticles; green) in the stratum corneum (sc), epidermis (ep), dermis (d) and hair follicle (hf).

membrane were determined, and the results are shown in Figure 1B. The accumulated amount of plasmid with PM was higher than that permeated in H_2O. To further compare the effect of particle size on the permeating profile, nanoparticles with two diameters (40, 100 nm) were performed. Figure 1C shows that the permeating rate of 40 nm nanoparticles was faster than that of 100 nm nanoparticles and was similar to the releasing profile of P/PM, indicating that the particle size affected the permeation rate.

Enhanced Transdermal Permeability of Plasmid after PM Formulation *in Vitro*. To evaluate whether polymer formulation increased the transdermal permeability of pCMV-*Lac* Z, skin of nude mice was used for *in vitro* permeation study. Results in Table 1 show that the calculated apparent permeability coefficients (P_{app}) of pCMV-*Lac* Z formulated with 0.01 or 0.1% of polymer were similar to that of pCMV-*Lac* Z alone ($3.4 \pm 0.8 \times 10^{-11}$ cm/s). Upon formulation with 5% polymer, the P_{app} values of pCMV-*Lac* Z, however, were significantly increased to $11.2 \pm 2.7 \times 10^{-11}$ cm/s indicating that the polymer at concentration above its CMC enhanced the transdermal permeability of pCMV-*Lac* Z.

Transdermal Permeation of P/PM Involve Energy-Dependent Process. To delineate whether the transport of pCMV-*Lac* Z formulated with 5% PM through skin was energy-dependent, the dependence on direction and temperature of transport were examined. The results (Table 2) showed that the P_{app} value of P/PM from the dermis to the stratum corneum was significantly decreased compared with that of P/PM permeated from the stratum corneum to the dermis (Table 2), demonstrating that the transport of P/PM was direction-dependent. However, the P_{app} value of the plasmid alone was no different in both directions. In addition, the P_{app} of P/PM was significantly decreased at lower temperatures (20 and 4 °C) compared with that permeated at 37 °C (Table 2), suggesting the temperature-dependence of P/PM permeating in the stratum corneum to the dermis. Furthermore, preadding 150 mM sodium azide, an inhibitor of the ATP synthesis, to skin caused the P_{app} values of plasmid and P/PM to be all inhibited and further supported that the permeation may involve an energy-dependent process. Meanwhile, there was no difference in P_{app} of pCMV-*Lac* Z alone permeated between 37 and 20 °C.

To compare permeation of solid nanoparticles on skin, 40 nm nanoparticles with zeta potential of -47.7 ± 5.7 mV were also studied. Results (Table 2) showed that the P_{app} of 40 nm nanoparticles was also observed to similarly decrease from the dermis to the stratum corneum direction compared with that of 40 nm nanoparticles permeated from the stratum corneum to the dermis. It was also significantly decreased at both 20 and 4 °C compared with that permeated at 37 °C, suggesting the energy-dependence of permeation of 40 nm nanoparticles. Furthermore, pretreatment with 150 mM sodium azide also inhibited permeation of nanoparticles in skin.

Additionally, after *in vitro* skin permeation of 40 nm nanoparticles, cryosections of permeated skins were analyzed by laser confocal microscope to observe the distribution of the solid nanoparticles. The results (Figure 2) showed that 40 nm nanoparticles were observed in stratum corneum, epidermis and dermis of the permeated skin, evidencing that 40 nm nanoparticles penetrated the stratum corneum and epidermis of skin and entered the dermis of skin.

Increased Permeation and Circulation Time of Plasmid with PM Formulation *in Vivo*. Owing to the increased transdermal permeability of plasmid by PM formulation, the pharmacokinetics of P/PM topically applied to nude mice with 48 h was studied. The results (Figure 3)

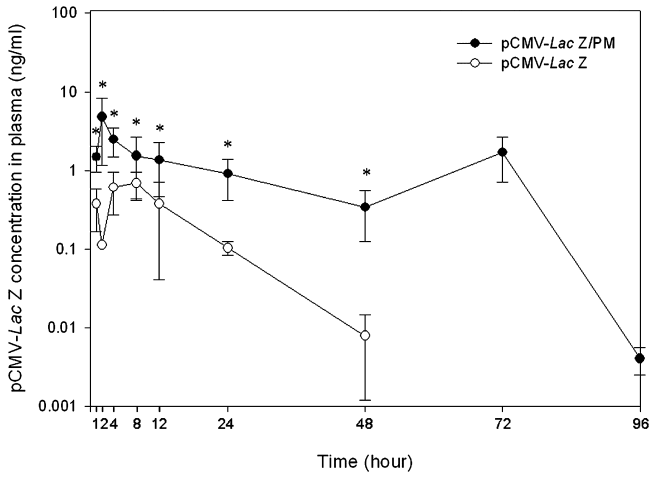

Figure 3. Plasma concentration−time profiles of pCMV-*Lac* Z with PM. BALB/cAnN.Cg-*Foxn1nu*/CrlNarl nude mice (6 to 8 weeks old) were topically administrated with pCMV-*Lac* Z or pCMV-*Lac* Z/PM on the abdominal side of skin within 48 h. After administration, blood was sampled from cannulated jugular vein at each time point (1, 2, 4, 8, 12, 24, 48, 72, 96, and 120 h postadministration) and DNA levels in plasma were measured by real-time PCR. The results are expressed as the mean ± SEM (N = 5−7). *: Significant different (P < 0.05) compared with pCMV-*Lac* Z at the same time point.

dx.doi.org/10.1021/mp200342h | *Mol. Pharmaceutics* 2012, 9, 111−120

Table 3. The β-Galactosidase Activity in Tissues of Mice Topically Receiving pCMV-*Lac* Z or pCMV-*Lac* Z/PM[a]

	β-Gal act. (RLU/mg protein)				
		pCMV-*Lac* Z	pCMV-*Lac* Z/PM		
	control	48 h	48 h	72 h	96 h
skin	10.6 ± 4.3	18.4 ± 4.5	212.6 ± 28.9[b,c,d,e]	113.3 ± 38.9[b,c,e]	38.1 ± 8.9
liver	2.6 ± 0.6	2.7 ± 0.5	3.1 ± 0.7	3.5 ± 0.7	2.3 ± 0.5
heart	32.1 ± 5.8	29.8 ± 4.0	31.6 ± 9.1	34.4 ± 3.2	28.5 ± 5.8
lung	26.5 ± 6.8	29.1 ± 4.3	25.9 ± 6.5	30.2 ± 9.0	31.8 ± 7.2
stomach	55.5 ± 18.0	68.3 ± 25.5	283.2 ± 36.3[b,c,d,e]	190.4 ± 43.4[b,c,e]	84.6 ± 19.4
duodenum	37.8 ± 11.8	41.2 ± 18.3	37.9 ± 15.8	36.4 ± 22.7	41.5 ± 7.8
spleen	39.0 ± 6.7	45.6 ± 4.8	47.3 ± 2.1	100.1 ± 10.3[b,c,e,f]	50.4 ± 6.0
kidney	19.6 ± 4.5	24.4 ± 1.8	21.8 ± 6.9	25.1 ± 8.2	24.1 ± 2.6
testis	55.6 ± 10.9	56.5 ± 6.8	71.4 ± 10.0	184.0 ± 35.3[b,c,e,f]	67.6 ± 9.7
brain	33.7 ± 8.9	45.2 ± 14.3	166.7 ± 25.1[b,c,e]	140.5 ± 18.1[b,c,e]	48.0 ± 7.3
spinal cord	48.3 ± 12.7	67.5 ± 20.2	177.5 ± 34.4[b,c,e]	159.5 ± 20.5[b,c,e]	68.8 ± 10.9

[a]BALB/cAnN.Cg-*Foxn1nu*/CrlNarl nude mice were topically administered with pCMV-*Lac* Z solution or pCMV-*Lac* Z/PM (100 μL of 0.4 μg/μL in H_2O or 5% PM) on abdominal skin. Tissues were excised at 48, 72, or 96 h after topical application. β-Galactosidase (β-Gal) activity (RLU/mg protein; $N = 6$) was expressed as mean and SEM. [b]Significant increase ($P < 0.05$) compared with control group. [c]Significant increase ($P < 0.05$) compared with pCMV-*Lac* Z 48 h. [d]Significant increase ($P < 0.05$) compared with pCMV-*Lac* Z/PM 72 h. [e]Significant increase ($P < 0.05$) compared with pCMV-*Lac* Z/PM 96 h. [f]Significant increase ($P < 0.05$) compared with pCMV-*Lac* Z/PM 48 h.

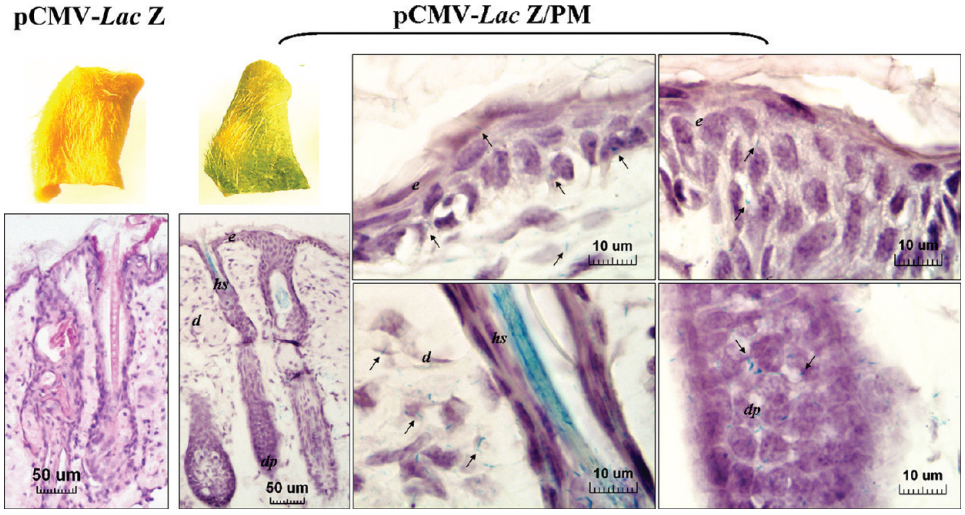

Figure 4. The whole-mount and histochemical analysis (X-Gal staining) of skin of nude mice after administration of pCMV-*Lac* Z and pCMV-*Lac* Z/PM. Skin was sampled at 48 h after pCMV-*Lac* Z or pCMV-*Lac* Z/PM administration. All the images of histological cryosections were counterstained with hematoxylin−eosin. Note the blue-green staining corresponding to β-Gal activity indicated by the arrows and observed in the epidermis (e), dermis (d), hair shaft (hs) and dermal papilla (dp). No inflammatory reaction was noted after pCMV-*Lac* Z/PM delivery.

showed that pCMV-*Lac* Z was detected in plasma starting early at 1 h, peaked at 2 h and continued to be detectable at 96 h postapplication of P/PM, while the peak level of plasmid was at 4−8 h and there was no detectable amount of plasmid DNA in plasma after 48 h application of pCMV-*Lac* Z alone. The calculated area under the curve ($AUC_{0\rightarrow\infty}$) of plasmid in P/PM application was about 10-fold ($AUC_{P/PM}$: 98.34 h·ng/mL) higher than that detected in mice applied with pCMV-*Lac* Z alone (AUC_P: 10.12 h·ng/mL); the half-life of pCMV-*Lac* Z was also increased from 6.46 to 11.34 h upon formulation with PM.

The Expression of *Lac* Z Delivered in PM Formulation *via* Transdermal Application. To demonstrate the delivered gene expression *in vivo*, measurement of β-Gal enzymatic activity in tissues including skin, liver, heart, lung, stomach, duodenum, spleen, kidney, testis, brain and spinal cord after P/PM transdermal application was performed. Results (Table 3) showed that significant increase of the β-Gal activity in skin was detected at 48, 72, and 96 h after P/PM application (212.6 ± 28.9, 113.3 ± 38.9 and 38.1 ± 8.9 RLU/mg for 48, 72, and 96 h respectively, compared with 10.6 ± 4.3 RLU/mg for the control group, $P < 0.05$), indicating the success of plasmid penetrating the skin and expressing the encoded protein. Similar results were detected in stomach (283.2 ± 36.3 and 190.4 ± 43.4 RLU/mg for 48 and 72 h compared with 55.5 ± 18.0 RLU/mg for the control group, $P < 0.05$), brain (166.7 ± 25.1 and 140.5 ± 18.1 RLU/mg for 48 and 72 h compared with 33.7 ± 8.9 RLU/mg for the control group, $P < 0.05$) and spinal cord (177.5 ± 34.4 and 159.5 ± 20.5 RLU/mg for 48 and 72 h compared with 48.3 ± 12.7 RLU/mg for the control group, $P < 0.05$) of mice receiving P/PM. The β-Gal activities were also significantly increased in spleen (100.1 ± 10.3 RLU/mg for P/PM, 39.0 ± 6.7 RLU/mg for control group, $P < 0.05$) and testis (184.0 ± 35.3 RLU/mg for P/PM, and 55.6 ± 10.9 RLU/mg for control group, $P < 0.05$) at 72 h postapplication of P/PM. There was no significance in β-Gal activity in other tested

dx.doi.org/10.1021/mp200342h | *Mol. Pharmaceutics* 2012, 9, 111−120

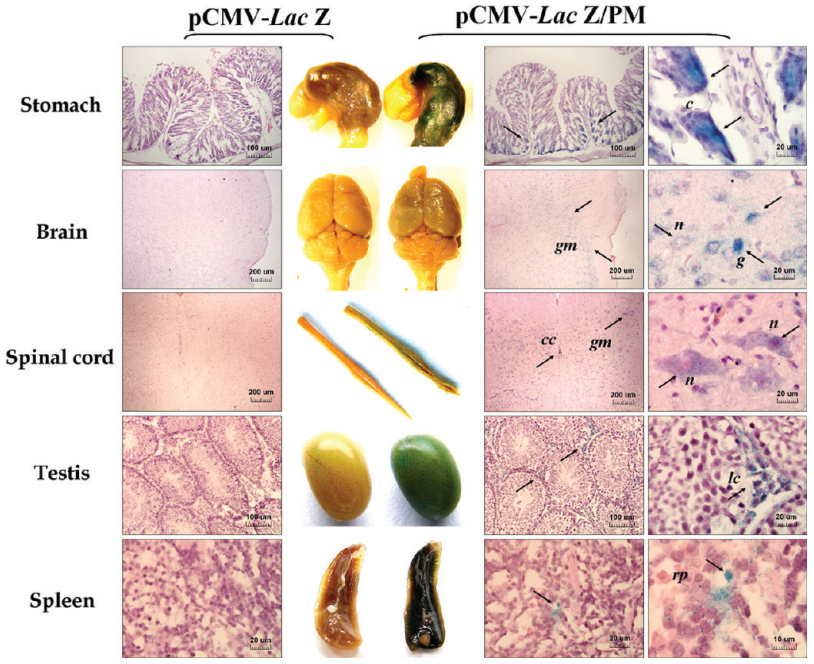

Figure 5. The whole-mount and histochemical analysis (X-Gal staining) of stomach, brain, spinal cord, testis and spleen of nude mice after administration of pCMV-*Lac* Z and pCMV-*Lac* Z/PM. Stomach, brain and spinal cord were sampled at 48 h after pCMV-*Lac* Z or pCMV-*Lac* Z/PM administration, and testis and spleen were sampled at 72 h postadministration. All the images of histological cryosections were counter-stained with hematoxylin−eosin. Note the blue-green staining corresponding to β-Gal activity indicated by the arrows and observe chief cells (c), central canal (cc), gray matter (gm), glial cells (g), neuron cells (n), red pulp (rp) and Leydig cells (lc). No inflammatory reaction was noted after pCMV-*Lac* Z/PM delivery.

tissues of mice receiving pCMV-*Lac* Z alone at 48 h (Table 3) and even 72 h (data not shown) postapplication compared to the control group (Table 3).

To further histologically localize the β-Gal activity, X-Gal staining in whole-mount and cryosections of tissues from mice receiving pCMV-*Lac* Z or P/PM was performed. Results (Figure 4) showed that the β-Gal activity was found in the epidermis, dermis, hair follicle, hair shaft, dermal papilla and sebaceous gland of skin. The β-Gal activity was also observed in the chief cells of gastric mucosa in stomach, glial cells and neuron cells in the gray matter of the brain and spinal cord, interstitial endocrinocyte (Leydig cell) of the testis and in the red pulp of the spleen (Figure 5). No such endogenous β-Gal activity was detected in any tissues. In addition, no toxic or inflammatory responses were observed by microscopic examination in all the tissues or animals during the entire study period.

DISCUSSION

The enhanced permeation of plasmid with PM by an *in vitro* release method using a cellulose membrane was observed (Figure 1B). Additionally, the average particle size of pCMV-*Lac* Z plasmid (66.8 ± 3.5 nm) was significantly decreased to the range of 47.6−51.1 nm upon P/PM formulation which has a similar permeation profile of 40 nm nanoparticles (Figures 1B and 1C). Regarding the particle size of the solid particles, a significant reduction in the percentage transport was seen after incubation with nonflexible 100 nm nanoparticles (Figure 1C), suggesting the particle size may affect the permeation in 0.2 μm pores of cellulose membrane. These may indicate that a complex of plasmid upon formulation with PM could influence the entrance into cellulose membrane as well as in the stratum corneum within 44 nm of intercellular space.[31] Recently, polyethylene glycol (PEG)-coated quantum dots (QDs) with particle size of 45 nm or PEG-containing nanoparticles with size of 40 nm were shown to penetrate through the stratum corneum and localize primarily in the epidermis or in some hair follicle.[32,33] These results were consistent with our observation of the distribution of 40 nm nanoparticles in skin (Figure 2). However, the apparent permeability coefficients of mouse skin differed between P/PM and 40 nm solid nanoparticles which both contained a similar range of particle size and zeta potential. Unlike solid particles or electrostatic complexes formed between cationic carriers and DNA, it had been reported that the P/PM complexes are likely to be formed by weak/low interactions, such as hydrogen bonds or ion-dipole between DNA and the poly(ethylene) oxide (PEO) corona part of PEO-PPO-PEO polymeric micelles.[34−36] Therefore, due to the weak/low interaction between plasmid and PM, plasmid could be affecting the stability of PM during penetration in the skin layers as well as enzyme degradation.

On the other hand, using noninvasive flexible carriers, liposome or transfersome, to deliver compounds with large molecular weight (interferon, insulin or bleomycin) could penetrate into stratum corneum and epidermis layer by interaction of intercellular lipids,[13] increase distribution of compound in epidermis and dermis,[37−39] and even transport therapeutic compound into the body.[37] It has been demonstrated that PEO-PPO-PEO triblock copolymer was taken up into cells *via* a receptor-mediated endocytotic mechanism that can be abolished at low temperature.[19,28] In addition, we previously found that uptake of these PEO polymeric micelle coronas in cultured cells or the entry of PM-mediated delivery of plasmid to duodenum *in vitro* and cornea *in vivo* possibly involved a receptor-mediated, temperature-dependent process.[22,26] This finding is consistent with our

results that P/PM delivery of plasmid to skin was influenced by temperature, sodium azide, and reversed transport (Table 2). Moreover, it has been reported that uptake of quantum dots (QDs) at particle sizes of 12−45 nm in primary human neonatal epidermal keratinocytes involved endocytosis and was decreased at 4 °C.[40,41] This observation is similar to our results that 40 nm nanoparticles permeated the intact skin may involve energy-dependent process (Table 2). Considering the average 50 nm size of plasmid upon formulation with PM in this study, it is likely that entry of this P/PM *via* skin may not only penetrate through stratum corneum within 44 nm of intercellular space but also involve endocytosis. However, the detailed nanoentry mechanisms on different cell types or layers of P/PM through the skin and stability of P/PM in the skin still need more investigation.

In our *in vivo* pharmacokinetic data of plasmid with PM increased the AUC of the plasmid and prolonged the half-life (Figure 3). These could be supported by PM, which has been reported to enhance the bioavailability of drugs and genes,[21−26] protect the plasmid to be more resistant to DNase digestion *in vitro*,[22] and reduce clearance of plasmid by the reticuloendothelial system (RES).[42,43] Using PEO/PPO block copolymer for surface modification of nanoparticles, there were also reports that it minimizes interactions with blood components and liver macrophage uptake.[44,45] In addition, the absolute bioavailability of the PM-delivered plasmid was estimated to be 6.61% ($AUC_{P/PM}$: 98.34 h·ng/mL; 40 μg of plasmid) referenced with the 11150.4 h·ng/mL AUC of plasmid intravenously administered at a 300 μg amount,[8] and this P/PM formulation increased ∼37-fold (0.18%) of that of plasmid applied transdermally at a 300 μg amount.[8] This nanosized PM of PEO-PPO-PEO may, therefore, serve as a transdermal carrier for systemic distribution of plasmid DNA.

Moreover, histological localization of transgene expressed cells within the skin revealed that the X-Gal positive cells were distributed in the epidermis, dermis, hair follicle, dermal papilla and sebaceous gland (Figure 4). The level of transgene expression (β-Gal activity; Table 3) in skin detected at 48 h postapplication in this study was similar to that obtained by liposome-mediated administration.[1,3] In addition, the expression pattern of β-Gal activity was found earlier (48 h) in higher blood flow organs (stomach, brain and spinal cord) and at 72 h in lower blood flow organs (spleen and testis). It has been reported that this copolymer increased drug entry to the bovine brain microvessel endothelial cell (BBMEC) possibly through the alterations of membrane structure, microviscosity and the P-glycoprotein efflux system, resulting in enhanced absorption and permeability of drugs.[19,28,46] We also have reported that this copolymer improved the bioavailability of small molecules, such as methylprednisolone (MP) in both plasma and spinal cord,[23] supporting the observation here of the detected *Lac* Z expression in brain and spinal cord in the P/PM group in this study. In addition, gold nanoparticles with smaller sizes of 15 and 50 nm were able to pass through the blood−brain barrier,[47] further supporting that the P/PM with particle size (51.1 ± 6.3 nm) is capable of expressing transgene in brain and spinal cord.[8,9]

Low X-Gal activity was found at the liver organ in our P/PM transdermal delivery, and the results of other researchers in pharmacokinetic studies showed that Pluronic micelles were accumulated at the liver organs.[48−50] However, several reports had suggested that gene expression efficiency may not correlate with the pattern of plasmid distribution.[51−53] These reports showed that even liver tissue had high percentage of transgene in tissues, but overall transgene activity was low compared to that detected in other organs. They suggested that this may be due to faster degradation of transgene occurring in liver.[51,52] In addition, the different compositions of Pluronic block copolymers have been suggested to affect the distribution and stability of delivered plasmids/drugs.[48−50] Therefore, plasmid could be affected the stability with PM during distribution in the liver tissues as well as transgene activity.

In conclusion, the transdermal permeability of plasmid was enhanced by PM-formulation and the PM-mediated transdermal penetration of plasmid may involve a direction- and temperature-dependent process. With this nano-PM, a nonviral delivery carrier, we detected a higher plasmid concentration (AUC) and longer half-life and globally distributed transgene expression at least for 3 days in skin, stomach, testis, spleen, and even the distant organs like brain and spinal cord.

AUTHOR INFORMATION

Corresponding Author

*College of Pharmacy, Taipei Medical University, 250 Wu Hsing St., Taipei 110, Taiwan. E-mail: jhorng@tmu.edu.tw. Tel: +886-2-2377-9873. Fax: +886-2-2377-9873.

ACKNOWLEDGMENTS

This work was supported by the National Science Council, Taipei, Taiwan (NSC-100-2320-B038-005).

REFERENCES

(1) Alexander, M. Y.; Akhurst, R. J. Liposome-mediated gene transfer and expression *via* the skin. *Hum. Mol. Genet.* **1995**, *4*, 2279−2285.
(2) Li, L.; Hoffman, R. M. The feasibility of targeted selective gene therapy of the hair follicle. *Nat. Med.* **1995**, *1*, 705−706.
(3) Raghavachari, N.; Fahl, W. E. Targeted gene delivery to skin cells *in vivo*: a comparative study of liposomes and polymers as delivery vehicles. *J. Pharm. Sci.* **2002**, *91*, 615−622.
(4) Ciernik, I. F.; Krayenbuhl, B. H.; Carbone, D. P. Puncture-mediated gene transfer to the skin. *Hum. Gene Ther.* **1996**, *7*, 893−899.
(5) Williams, R. S.; Johnston, S. A.; Riedy, M.; DeVit, M. J.; McElligott, S. G.; Sanford, J. C. Introduction of foreign genes into tissues of living mice by DNA-coated microprojectiles. *Proc. Natl. Acad. Sci. U.S.A.* **1991**, *88*, 2726−2730.
(6) Zhang, L.; Li, L.; Hoffman, G. A.; Hoffman, R. M. Depth-targeted efficient gene delivery and expression in the skin by pulsed electric field: an approach to gene therapy of skin aging and other diseases. *Biochem. Biophys. Res. Commun.* **1996**, *220*, 633−636.
(7) Udvardi, A.; Kufferath, I.; Grutsch, H.; Zatloukal, K.; Volc-Platzer, B. Uptake of exogenous DNA *via* the skin. *J. Mol. Med.* **1999**, *77*, 744−750.
(8) Kang, M. J.; Kim, C. K.; Kim, M. Y.; Hwang, T. S.; Kang, S. Y.; Kim, W. K.; Ko, J. J.; Oh, Y. K. Skin permeation, biodistribution, and expression of topically applied plasmid DNA. *J. Gene Med.* **2004**, *6*, 1238−1246.
(9) Dokka, S.; Cooper, S. R.; Kelly, S.; Hardee, G. E.; Karras, L. G. Dermal delivery of topically applied oligonucleotides *via* follicular transport in mouse skin. *J. Invest. Dermatol.* **2005**, *123*, 971−975.
(10) Domashenko, A.; Gupta, S.; Cotsarelis, G. Efficient delivery of transgenes to human hair follicle progenitor cells using topical lipoplex. *Nat. Biotechnol.* **2000**, *18*, 420−423.
(11) Hadgraft, J. Modulation of the barrier function of the skin. *Skin Pharmacol. Appl. Skin Physiol.* **2001**, *14* (Suppl. 1), 72−81.
(12) Li, L.; Hoffman, R. M. Topical liposome delivery of molecules to hair follicles in mice. *J. Dermatol. Sci.* **1997**, *14*, 101−108.
(13) Foldvari, M.; Badae, I.; Wettig, S.; Baboolal, D.; Kumar, P.; Creagh, A. L.; Haynes, C. A. Topical delivery of interferon alpha by

biphasic vesicles: evidence for a novel nanopathway across the stratum corneum. *Mol. Pharmaceutics* **2010**, *7*, 751−762.
(14) Prokop, A.; Kozlov, E.; Moore, W.; Davidson, J. M. Maximizing the *in vivo* efficiency of gene transfer by means of nonviral polymeric gene delivery vehicles. *J. Pharm. Sci.* **2002**, *91*, 67−76.
(15) Raghavan, S. L.; Kiepfer, B.; Davis, A. F.; Kazarian, S. G.; Hadgraft, J. Membrane transport of hydrocorticone acetate from supersaturated solutions; the role of polymers. *Int. J. Pharm.* **2001**, *221*, 95−105.
(16) Takahashi, A.; Suzuki, S.; Kawasaki, N.; Kubo, W.; Miyazaki, S.; Loebenberg, R.; Bachynsky, J.; Attwood, D. Percutaneous absorption of non-steroidal anti-inflammatory drugs from *in situ* gelling xyloglucan formulations in rats. *Int. J. Pharm.* **2002**, *246*, 179−186.
(17) Yalin, M.; Oner, F.; Oner, L.; Hincal, A. A. Preparation and properties of a stable intravenous lorazepam emulsion. *J. Clin. Pharm. Ther.* **1997**, *22*, 39−44.
(18) Kabanov, A. V.; Batrakova, E. V.; Alakhov, V. Y. Pluronic block copolymers as novel polymer therapeutics for drug and gene delivery. *J. Controlled Release* **2002**, *82*, 189−212.
(19) Batrakova, E. V.; Li, S.; Miller, D. W.; Kabanov, A. V. Pluronic P85 increases permeability of a broad spectrum of drugs in polarized BBMEC and Caco-2 cell monolayers. *Pharm. Res.* **1999**, *16*, 1366−1372.
(20) Thuret, G.; Manissolle, C.; Campos-Guyotat, L.; Guyotat, D.; Gain, P. Animal compound-free medium and poloxamer for human corneal organ culture and dewelling. *Invest. Ophthalmol. Vis. Sci.* **2005**, *46*, 816−822.
(21) Tong, Y. C.; Chang, S. F.; Kao, W. W.-Y.; Liu, C. Y.; Liaw, J. Polymeric micelle gene delivery of bcl-x_L *via* eye drop reduced corneal apoptosis following epithelial debridement. *J. Controlled Release* **2010**, *147*, 76−83.
(22) Tong, Y. C.; Chang, S. F.; Liu, C. Y.; Kao, W. W.-Y.; Huang, C. H.; Liaw, J. Eye drop delivery of nano-polymeric micelle formulated genes with cornea-specific promoters. *J. Gene Med.* **2007**, *9*, 956−966.
(23) Chen, C. L.; Chang, S. F.; Lee, D.; Yang, L. Y.; Lee, Y. H.; Hsu, C. Y.; Lin, S. J.; Liaw, J. Bioavailability effect of methylprednisolone by polymeric micelle. *Pharm. Res.* **2008**, *25*, 39−47.
(24) Liaw, J.; Lin, Y. C. Evaluation of poly(ethylene oxide)-poly(propylene oxide)-poly(ethylene oxide) (PEO-PPO-PEO) gels as a release vehicle for percutaneous fentanyl. *J. Controlled Release* **2000**, *68*, 273−282.
(25) Kwon, S. H.; Kim, S. Y.; Ha, K. W.; Kang, M. J.; Huh, J. S.; Im, T. J.; Kim, Y. M.; Park, Y. M.; Kang, K. H.; Lee, S.; Chang, J. Y.; Lee, J.; Choi, Y. W. Pharmaceutical evaluation of genistein-loaded Pluronic micelles for oral delivery. *Arch. Pharmacal Res.* **2007**, *30*, 1138−1143.
(26) Chang, S. F.; Chang, H. Y.; Tong, Y. C.; Chen, S. H.; Hsaio, F. C.; Lu, S. C.; Liaw, J. Nonionic polymeric micelles for oral gene delivery *in vivo*. *Hum. Gene Ther.* **2004**, *15*, 481−493.
(27) MacGregor, G. R.; Caskey, C. T. Construction of plasmids that express E. coli *β*-galactosidase in mammalian cells. *Nucleic Acids Res.* **1989**, *17*, 2365−2369.
(28) Liaw, J.; Aoyagi, T.; Kataoka, K.; Sakurai, Y.; Sakurai, Y.; Okano, T. Permeation of PEO-PBLA-FITC polymeric micelles in aortic endothelial cells. *Pharm. Res.* **1999**, *16*, 213−220.
(29) Nesti, E.; Everill, B.; Morielli, A. D. Endocytosis as a mechanism for tyrosine kinase-dependent suppression of a voltage-gated potassium channel. *Mol. Biol. Cell* **2004**, *15*, 4073−4088.
(30) Oka, J. A.; Christensen, M. D.; Weigel, P. H. Hyperosmolarity inhibits galactosyl receptor-mediated but not fluid phase endocytosis in isolated rat hepatocytes. *J. Biol. Chem.* **1989**, *264*, 12016−12024.
(31) Al-Amoudi, A.; Dobochet, J.; Norlén, L. Nanostructure of the epidermis extracellular space as observed by cryo-electron microscopy of vitreous sections of human skin. *J. Invest. Dermatol.* **2005**, *124*, 764−777.
(32) Ryman-Rasmussen, J. P.; Riviere, J. E.; Monteiro-Riviere, N. A. Penetration of intact skin by quantum dots with diverse physicochemical properties. *Toxicol. Sci.* **2006**, *91*, 159−165.
(33) Shim, J.; Seok, K. H.; Park, W. S.; Han, S. H.; Kim, J.; Chang, I. S. Transdermal delivery of minoxidil with block copolymer nanoparticles. *J. Controlled Release* **2004**, *97*, 477−484.
(34) Lemieux, P.; Guérin, N.; Paradis, G.; Proulx, R.; Chistyakova, L.; Kabanov, A.; Alakhov, V. Acombination of poloxamers increases gene expression of plasmid DNA in skeletal muscle. *Gene Ther.* **2000**, *7*, 986−911.
(35) Alimi-Guez, D.; Leborgne, C.; Pembouong, G.; Van Wittenberghe, L.; Mignet, N.; Scherman, D.; Kichler, A. Evaluation of the muscle gene transfer activity of a series of amphiphilic triblock copolymers. *J. Gene Med.* **2009**, *11*, 1114−1124.
(36) Huang, C. Y.; Ma, S. S.; Lee, S.; Radhakrishnan, R.; Braun, C. S.; Choosakoonkriang, S.; Wiethoff, C. M.; Lobo, B. A.; Middaugh, C. R. Enhancements in gene expression by the choice of plasmid DNA formulations containing neutral polymeric excipients. *J. Pharm. Sci.* **2002**, *91*, 1371−1381.
(37) Cevc, G.; Gebauer, D.; Stieber, J.; Schätzlein, A.; Blume, G. Ultraflexible vesicles, Transfersomes, have an extremely low pore penetration resistance and transport therapeutic amounts of insulin across the intact mammalian skin. *Biochim. Biophys. Acta* **1998**, *1368*, 201−215.
(38) Wachter, C.; Vierl, U.; Cevc, G. Adaptability and elasticity of the mixed lipid bilayers vesicles containing non-ionic surfactant designed for targeted drug delivery across the skin. *J. Drug Targeting* **2008**, *16*, 611−625.
(39) Hiruta, Y.; Hattori, Y.; Kawano, K.; Obata, Y.; Maitani, Y. Novel ultra-deformable vesicles entrapped with bleomycin and enhanced to penetrate rat skin. *J. Controlled Release* **2006**, *113*, 146−154.
(40) Ryman-Rasmussen, J. P.; Riviere, J. E.; Monteiro-Riviere, N. A. Variables influencing interactions of untargeted quantum dot nanoparticles with skin cells and identification of biochemical modulators. *Nano Lett.* **2007**, *7*, 1344−1348.
(41) Zhang, L. W.; Monteiro-Riviere, N. A. Mechanisms of quantum dot nanoparticle cellular uptake. *Toxicol. Sci.* **2009**, *110*, 138−155.
(42) Owens, D. E. III; Peppas, N. A. Opsonization, biodistribution, and pharmacokinetics of polymeric nanoparticles. *Int. J. Pharm.* **2006**, *307*, 93−102.
(43) Kataoka, K.; Kwon, G. S.; Yokoyama, M.; Okano, T.; Sakurai, Y. Block copolymer micelles as vehicles for drug delivery. *J. Controlled Release* **1993**, *24*, 119−132.
(44) Tan, J. S.; Butterfield, D. E.; Voycheck, C. L.; Caldwell, K. D.; Li, J. T. Surface modification of nanoparticles by PEO/PPO block copolymers to minimize interactions with blood components and prolong blood circulation in rats. *Biomaterials* **1993**, *14*, 823−833.
(45) Gaur, U.; Sahoo, S. K.; De, T. K.; Ghosh, P. C.; Maitra, A.; Ghosh, P. K. Biodistribution of fluoresceinated dextran using novel nanoparticles evading reticuloendothelial system. *Int. J. Pharm.* **2000**, *20*, 1−10.
(46) Batrakova, E. V.; Li, S.; Vinogradov, S. V.; Alakhov, V. Y.; Miller, D. W.; Kabanov, A. V. Mechanism of Pluronic effect on P-glycoprotein efflux system in blood-brain barrier: contributions of energy depletion and membrane. *J. Pharmacol. Exp. Ther.* **2001**, *299*, 483−493.
(47) Sonavane, G.; Tomoda, K.; Makino, K. Biodistribution of colloidal gold nanoparticles after intravenous administration: effect of particle size. *Colloids Surf., B* **2008**, *66*, 274−280.
(48) Batrakova, E. V.; Li, S.; Li, Y.; Alakhov, V. Y.; Elmquist, W. F.; Kabanov, A. V. Distribution kinetics of a micelle-forming block copolymer Pluronic P85. *J. Controlled Release* **2004**, *100*, 389−397.
(49) Wang, Y.; Li, Y.; Zhang, L.; Fang, X. Pharmacokinetics and biodistribution of paclitaxel-loaded Pluronic P105 polymeric micelles. *Arch. Pharm. Res.* **2008**, *31*, 530−538.
(50) Han, L. M.; Guo, J.; Zhang, L. J.; Wang, Q. S.; Fang, X. L. Pharmacokinetics and biodistribution of polymeric micelles of paclitaxel with Pluronic P123. *Acta. Pharmacol. Sin.* **2006**, *27*, 747−753.
(51) Thierry, A. R.; Lunardi-Iskandar, Y.; Bryant, J. L.; Rabinovich, P.; Gallo, R. C.; Mahan, L. C. Systemic gene therapy: biodistribution and long-term expression of a transgene in mice. *Proc. Natl. Acad. Sci. U.S.A.* **1995**, *92*, 9742−9746.

(52) Osaka, G.; Carey, K.; Cuthbertson, A.; Godowski, P.; Patapoff, T.; Ryan, A.; Gadek, T.; Mordenti, J. Pharmacokinetics, tissue distribution, and expression efficiency of plasmid [33P]DNA following intravenous administration of DNA/cationic lipid complexes in mice: use of a novel radionuclide approach. *J. Pharm. Sci.* **1996**, *85*, 612−618.
(53) Liu, F.; Qi, H.; Huang, L.; Liu, D. Factors controlling the efficiency of cationic lipid-mediated transfection in vivo via intravenous administration. *Gene Ther.* **1997**, *4*, 517−523.